

## MIT Open Access Articles

*Large-area NbN superconducting nanowire avalanche photon detectors with saturated detection efficiency*

The MIT Faculty has made this article openly available. **Please share** how this access benefits you. Your story matters.

**Citation:** Murphy, Ryan P., Matthew E. Grein, Theodore J. Gudmundsen, Adam McCaughan, Faraz Najafi, Karl K. Berggren, Francesco Marsili, and Eric A. Dauler. "Large-Area NbN Superconducting Nanowire Avalanche Photon Detectors with Saturated Detection Efficiency." Edited by Mark A. Itzler and Joe C. Campbell. *Advanced Photon Counting Techniques IX* (May 13, 2015). © 2015 Society of Photo-Optical Instrumentation Engineers (SPIE)

**As Published:** <http://dx.doi.org/10.1117/12.2178322>

**Publisher:** SPIE

**Persistent URL:** <http://hdl.handle.net/1721.1/99751>

**Version:** Final published version: final published article, as it appeared in a journal, conference proceedings, or other formally published context

**Terms of Use:** Article is made available in accordance with the publisher's policy and may be subject to US copyright law. Please refer to the publisher's site for terms of use.



# Large-Area NbN Superconducting Nanowire Avalanche Photon Detectors with Saturated Detection Efficiency<sup>§</sup>

Ryan P. Murphy<sup>\*a</sup>, Matthew E. Grein<sup>a</sup>, Theodore J. Gudmundsen<sup>a</sup>, Adam McCaughan<sup>b</sup>, Faraz Najafi<sup>b</sup>, Karl K. Berggren<sup>b</sup>, Francesco Marsili<sup>c</sup>, Eric A. Dauler<sup>a</sup>

<sup>a</sup>Massachusetts Institute of Technology Lincoln Laboratory, 244 Wood Street, Lexington, MA, USA 02420;

<sup>b</sup>Massachusetts Institute of Technology, Research Laboratory of Electronics, 50 Vassar Street, Cambridge MA, USA 02139;

<sup>c</sup>Jet Propulsion Laboratory, 4800 Oak Grove Drive, Pasadena, CA, USA 91109

## ABSTRACT

Superconducting circuits comprising SNSPDs placed in parallel—superconducting nanowire avalanche photodetectors, or SNAPs—have previously been demonstrated to improve the output signal-to-noise ratio (SNR) by increasing the critical current. In this work, we employ a 2-SNAP superconducting circuit with narrow (40 nm) niobium nitride (NbN) nanowires to improve the system detection efficiency to near-IR photons while maintaining high SNR. Additionally, while previous 2-SNAP demonstrations have added external choke inductance to stabilize the avalanching photocurrent, we show that the external inductance can be entirely folded into the active area by cascading 2-SNAP devices in series to produce a greatly increased active area. We fabricated series-2-SNAP (s2-SNAP) circuits with a nanowire length of 20  $\mu\text{m}$  with cascades of 2-SNAPs providing the choke inductance necessary for SNAP operation. We observed that (1) the detection efficiency saturated at high bias currents, and (2) the 40 nm 2-SNAP circuit critical current was approximately twice that for a 40 nm non-SNAP configuration.

**Keywords:** Photodetector, Quantum-detector, Single-photon-detector, NbN-SNSPD, SNAP

## 1. INTRODUCTION

Superconducting Nanowire Single Photon Detectors (SNSPDs) have emerged as a leading technology for achieving high photon detection efficiency (PDE) for single-photons at high counting rates with low timing jitter and low dark count rates. While research on various nanowire materials is being actively pursued, at present the two leading material systems are based on WSi and NbN (or NbTiN), each with various advantages and disadvantages.<sup>1</sup> NbN-based nanowires have demonstrated the highest counting rates (or fast reset times) and lowest timing jitter compared to other materials.<sup>2</sup> WSi-based nanowires have demonstrated the highest system photon detection efficiency, (PDE  $\sim$  93%) at near-infrared wavelengths using relatively wide (120 nm) nanowires,<sup>3</sup> but require colder (typically  $< 1$  K) operation due to the lower critical temperature. It is believed that the amorphous nature of WSi thin films creates much larger photon-induced hotspots in a given cross sectional area compared to NbN or NbTiN, and that the larger hotspots contribute to improved internal efficiency (defined as the probability that an absorbed photon is detected) as evidenced in WSi.<sup>3</sup>

Reducing the cross-sectional dimensions of the nanowires can improve the internal efficiency in NbN,<sup>4,5</sup> but does so at the expense of critical current ( $I_C$ ) and SNR. SNAPs have been shown to improve the SNR of NbN SNSPDs.<sup>6</sup> Key to the operation of a SNAP is the design of an appropriate choke inductance to control the electro-thermal dynamics of the

---

\*ryan.murphy@ll.mit.edu; phone 1 (781) 981-8164; fax 1 (781) 981-9108; www.ll.mit.edu

<sup>§</sup>This work was sponsored by the Assistant Secretary of Defense for Research & Engineering under Air Force Contract number FA8721-05-C-0002. Opinions, interpretations, conclusions, and recommendations are those of the authors, and not necessarily endorsed by the United States Government.

superconducting detector circuit. In this work, we show an improved internal efficiency in NbN-based SNSPDs for 1550-nm photons using narrow nanowires, and further, we show a modified SNAP design that improves the SNR of the detection circuit featuring a choke inductor that, unlike previous s2-SNAP demonstrations to our knowledge,<sup>7,8</sup> comprised the entirety of the optically-active area.

## 2. CIRCUIT DESIGN

The equivalent circuit layout for the superconducting circuit is shown in Figure 1a. The basic 2-SNAP is constructed of two narrow (40-nm wide) parallel nanowires with inductance  $L_k$  in series with a choke inductance  $L_S$  and a load resistance  $R_L$ .  $L_S$  is comprised of nine identical 2-SNAPs, which has been shown to stabilize the electro-thermal circuit dynamics according to our simulations and experiments. In this geometry, each 2-SNAP divides the bias current equally in each branch, and an absorbed photon in any of the nanowires will, with the appropriate current bias, lead to an avalanching current in the parallel nanowire. The current will subsequently flow into the load resistor with twice the current compared to that using a single (non-parallel) nanowire of the same width. Since copies of the photosensitive 2-SNAP provide the additional inductance, the active area is enhanced in this case by a factor of ten. We call this a cascaded series-2-SNAP, or an s2-SNAP.

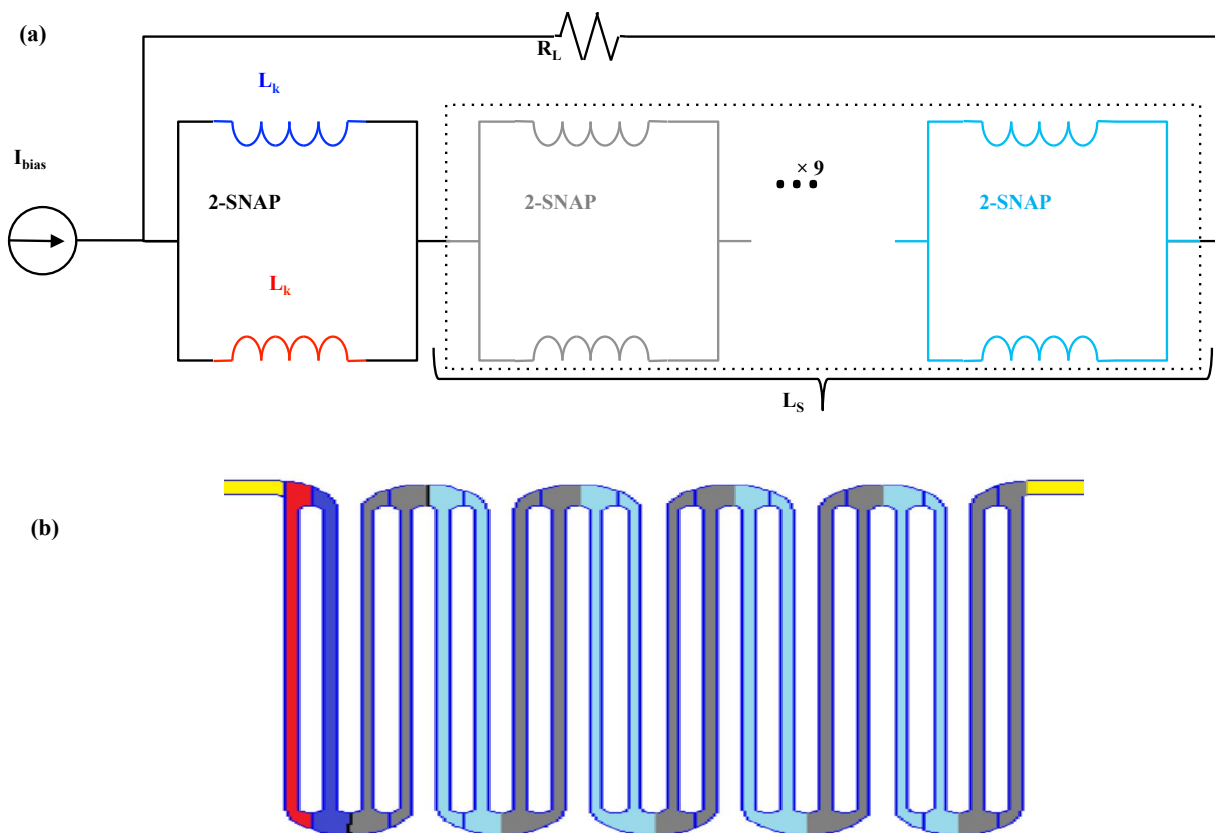


Figure 1. (a) Equivalent circuit for the s2-SNAP, where each nanowire is an inductor with kinetic inductance  $L_k$ . (b) Schematic of the s2-SNAP. The red and dark-blue elements comprise the base unit; the alternating gray and light-blue portions are copies of the base unit.

## 3. FABRICATION

The narrow nanowire devices were fabricated with e-beam lithography on 5-nm-thick NbN films (18.1% nitrogen concentration) on top  $\text{SiO}_2$ -on-Si substrates. The wire width, spacing between wires, and active area, defined as the total area covered by the nanowires, were 40 nm, 80 nm, and  $9.4 \mu\text{m}^2$ , respectively. The curvature of the bends between nanowire elements in parallel was designed to minimize current crowding (see Fig. 1b).<sup>9</sup> Before the nanowire devices were patterned in the e-beam system, platinum contact pads were fabricated to allow for electrical contact to the

detectors. After detector fabrication, a flowable oxide spacer and a thin gold mirror were fabricated on top, which acted as an optical cavity to enhance photon absorption in the nanowires.<sup>10</sup>

#### 4. MEASUREMENT

A customized semi-automated cryogenic probing system was used to test the optical efficiency of the s2-SNAPs. The nanowire devices fabricated on 4-inch wafers were diced into twelve 1-cm<sup>2</sup> chips, each having an assortment of 196 nanowire devices in an equally-spaced array across the chip. Up to seven 1-cm<sup>2</sup> chips can be mounted on to the sample holder, a gold-plated aluminum carousel with eight rimmed square frames (see Figure 2) by applying silver paint to establish thermal contact between the sample and one of the frames of the gold-plated holder. One of the frames holds a temperature sensor. Braided copper strands attached with indium solder connect the center of the carousel with a gold plated copper block and are placed in direct contact with the second stage anchor of the pulse-tube cryogenic system to thermalize the diced wafers with the ~2 K second stage anchor. The carousel is mounted to a four-axis stack (x, y, z,  $\theta$ ) of cryogenic piezo nano-positioners. A high-speed 40-GHz-bandwidth ground-signal-ground (G-S-G) electrical probe is mounted in a stationary position above the sample carousel in thermal contact to the second stage anchor. The  $\theta$ -axis of the four-axis stack of nano-positioners rotates so that any one of the seven chips can be positioned underneath the probe. The x- and y-axis positioners can maneuver the sample holder carousel to align the electrical contact pads with the G-S-G probe. The z-axis positioner can lift the carefully-positioned in x and y sample holder carousel up towards the probe to establish electrical contact with the detector. Light is coupled into the photodetector by passing attenuated light in a SMF-28 fiber through a cryogenic feed-through and focusing onto the nanowire detector active area with a focusing lens in a cryogenically compatible housing attached to the vacuum side of the SM fiber. The focusing lens is attached to an additional three-axis stack (x, y, z) of nano-positioners, nearly identical to those previously mentioned in the four-axis stack, and are used to position the fiber with the focusing assembly so that the light can be coupled into the nanowire structure on the chip.

An aluminum vacuum can encloses the entire cryogenic assembly. A Nickel-plated radiation shield attached to the first (~40 K) cryogenic stage encloses the second stage (~2 K) anchor of the cryogenic system as well as the sample chamber. A smaller gold-plated copper shield attached to the second stage anchor encloses the nanowire detectors on the sample holder, the high-speed electrical probe, the nano-positioners, and the fiber with the focuser housing to provide for additional shielding.

A high-resolution video camera and LED snake light on the outside of the cryogenic system point through optical windows in the vacuum can and both radiation shields at a mirror—mounted at 45 degrees on the top of the sample chamber, above the nanowire detectors and focusing lens—allowing in-situ visual imaging of the inside of the chamber (see Figure 3). The camera and the 4-axis nano-positioners interface with custom image recognition software written with MATLAB to control the nano-positioners so that each nanowire can sequentially be placed in electrical contact with the stationary high-speed electrical probe. Attenuated light from a pulsed 1550-nm laser was sent through a fiber-coupled splitter (for calibration purposes), polarizer (to align the electric field to the nanowires) and a vacuum feed through into the cryogenic system where the focusing lensed fiber assembly focused the light onto the detector active area in a 4.2- $\mu$ m-diameter spot. A bias current from a low-noise voltage source and series resistor was applied to the contact pads at the ends of the nanowire through the high-speed electrical probe. When the biased nanowire switched from its superconducting to resistive state, the current in the nanowire was shunted through a load resistor, and a voltage pulse was recorded. The RF signal passed out of the cryogenic system through a bias-tee to low-noise amplifiers and a comparator circuit before entering a time-correlated photon counter. With the exception of positioning of the focusing lens the system functioned in an automated mode with minimal user intervention.

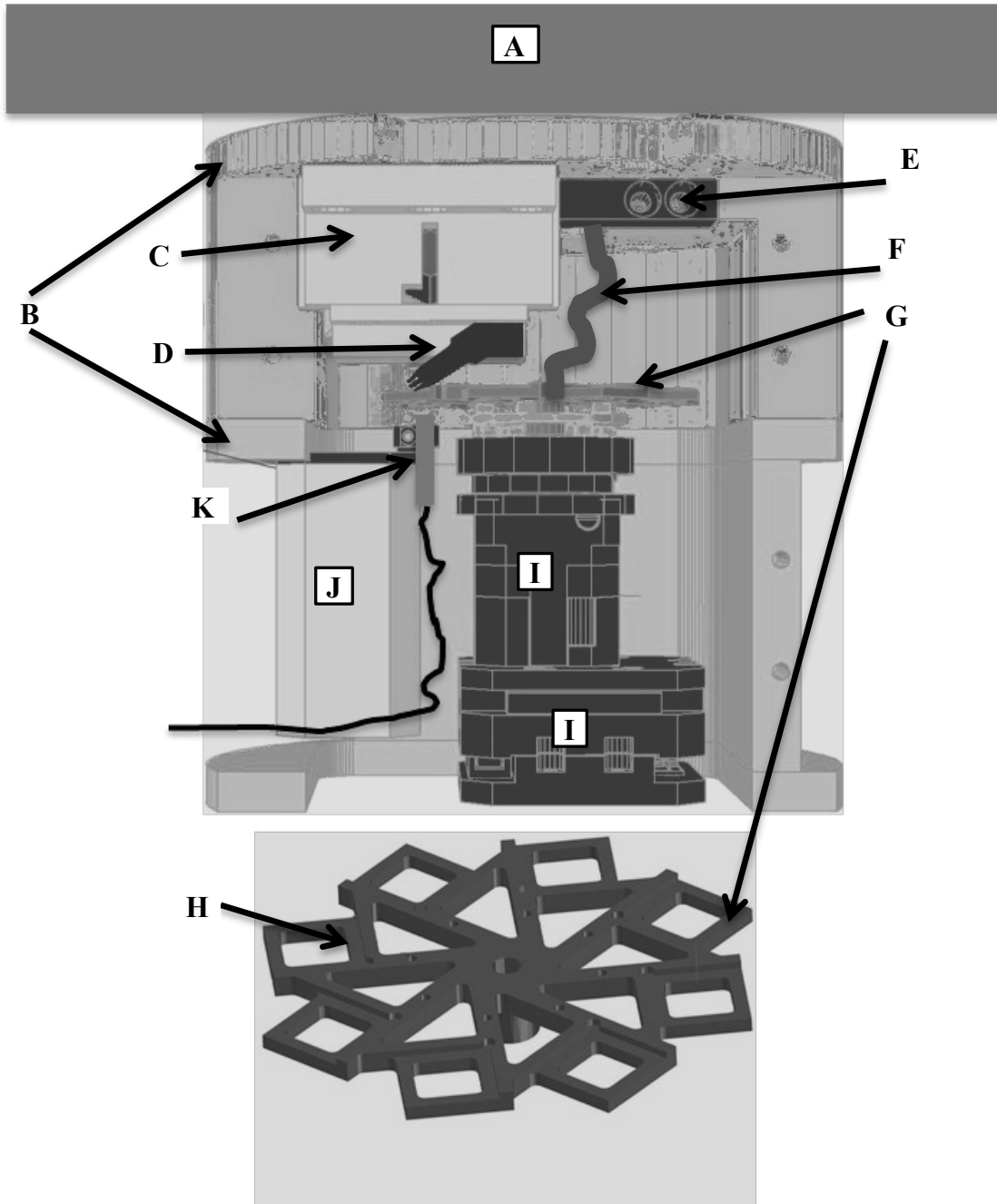


Figure 2. Cutaway CAD drawing of the semi-automated SNSPD probing system sample chamber, including (A) second-stage thermal anchor; (B) gold-plated copper radiation shield; (C) gold-plated copper mounting clamp for the high-speed electrical probe; (D) high-speed electrical probe; (E) gold-plated copper clamp for thermal syncing to the samples; (F) copper braided wire; (G) gold-plated aluminum sample holder; (H) chip holder rim for silver painting; (I) nano-positioners for sample carousel; (J) nano-positioners for focusing lenses; (K) cryogenic housing containing focusing lenses.

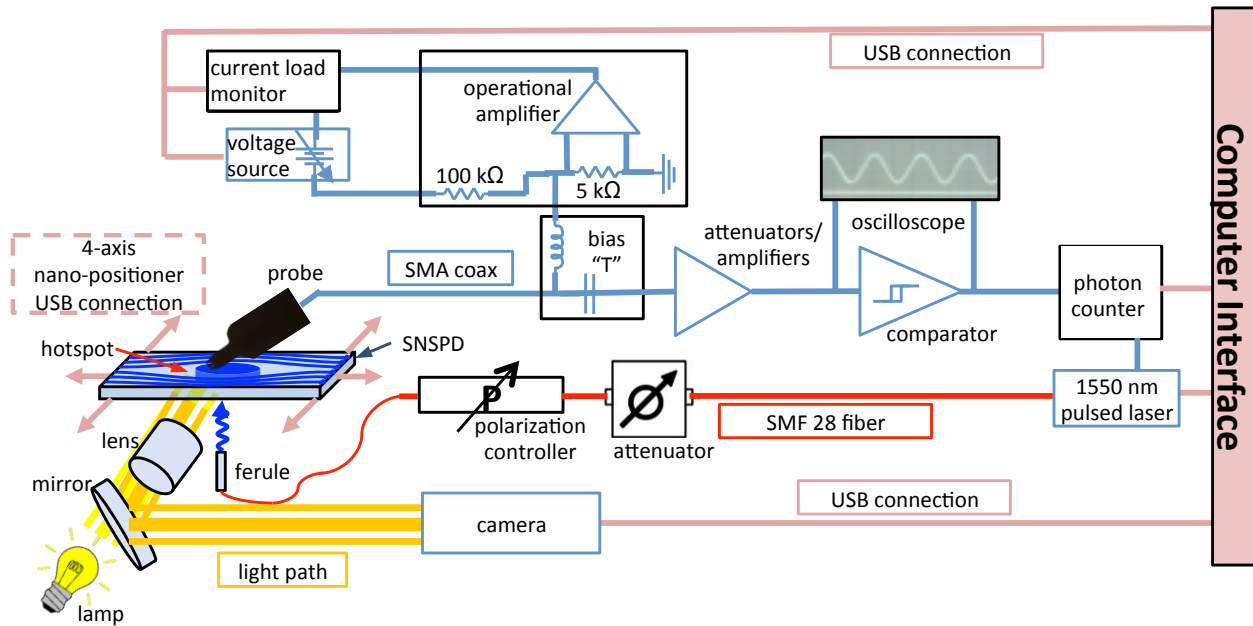


Figure 3. Measurement setup using the semi-automated probing system. Light from a 1550 nm pulsed source was sent through an attenuator, coupler (for calibration purposes), polarizer (to align the electric field coupling to the nanowires), and optical assembly positioned to focus the light onto the active area. A high-speed electrical probe made electric contact to the pads at the ends of the nanowires, which are biased by a low-noise voltage source. The RF signal passed through a bias-tee to low-noise amplifiers and a comparator circuit before entering a time-correlating photon counter.

## 5. RESULTS AND CONCLUSIONS

Figure 4 shows system PDE vs. bias current for the s2-SNAP. The system PDE includes the internal and absorption efficiency and is defined as the number of non-dark s2-SNAP counting events divided by the number of photons sent into the fiber just before the air-side end of the SM fiber. Counts measured without illuminating the s2-SNAP were subtracted from the counts measured while illuminating the s2-SNAP with 1550-nm photons to obtain the number of non-dark s2-SNAP counting events. The error bars in Figure 4 indicate the variance of results from identically designed devices, and a solid line is a phenomenological fit as a guide to the eye. Previous work has shown that increasing the switching current  $I_{SW}$  by a factor of two corresponds to increasing the SNR by the same factor.<sup>5</sup> For individual SNSPDs with 40-nm-wide wires  $I_{SW}$  ranges from 4-6  $\mu\text{A}$  (data not shown) while  $I_{SW}$  is  $\sim 11 \mu\text{A}$  for 40-nm-nanowire s2-SNAPs—almost twice as large and resulting in double the readout SNR. The clear PDE saturation at  $\sim 50\%$  near  $I_{SW}$  in Figure 4 is indicative of high internal efficiency.<sup>5</sup> Because the active area of the s2-SNAP is smaller than the spot size of the focused illumination beam, we have estimated the number of photons incident on the detector by using a Gaussian approximation and carefully accounting for optical loss. Given that the optical cavity for these s2-SNAPs was not optimized for 40-nm wire width and 80-nm wire-to-wire spacing, resulting in less photon absorption, we expect that the saturated PDE value can be increased through further fabrication development.

In summary, we have shown saturated PDE  $\sim 50\%$  in series-2-SNAPs with high SNR, indicating a robust design that should reach higher PDE with further optical cavity optimization. Furthermore we demonstrated the first (to our knowledge) saturated 2-SNAP that does not require a choke inductor outside the detector region. The two-fold SNR increase of s2-SNAPs over traditional SNSPDs may simplify implementing large arrays of SNSPDs by reducing required power to cryogenically amplify small detector signals, offering new opportunities for scalable, cryogenic readout electronics.

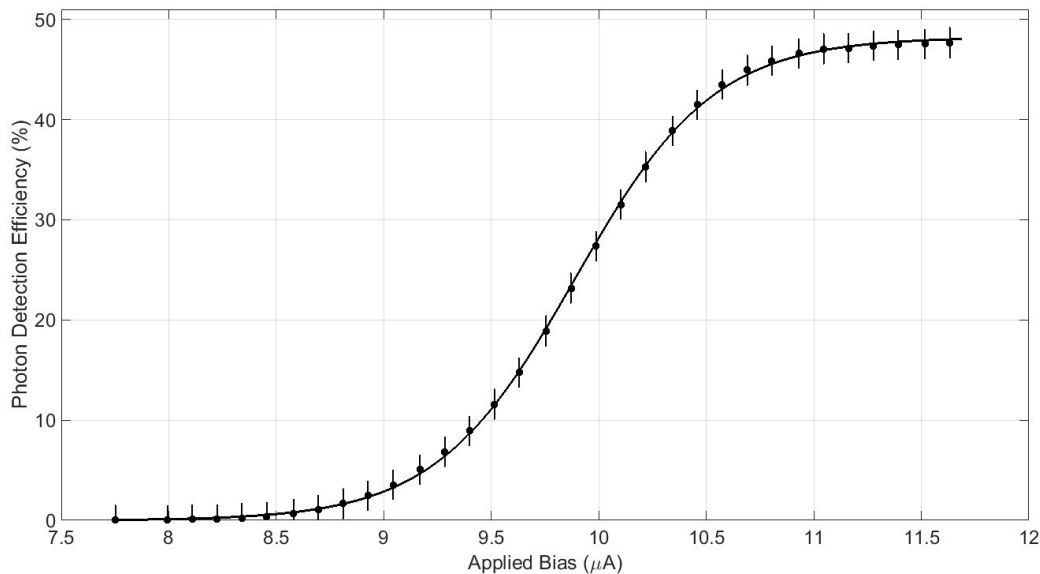


Figure 4. PDE vs. detector bias current for an s2-SNAP. Error bars indicate variance of results from measurements of identically designed s2-SNAPs.

## REFERENCES

- [1] Dauler, E. A., Grein, M. E., Kerman, A. J., Marsili, F., Miki, S., Nam, S. W., Shaw, M. D., Terai, H., Verma, V. B., Yamashita, T., "Review of superconducting nanowire single-photon detector system design options and demonstrated performance," *Opt. Eng.* 53(8), 081907-1-13 (2014).
- [2] Rosenberg, D., Kerman, A. J., Molnar, R. J., Dauler, E. A., "High-speed and high-efficiency superconducting nanowire single photon detector array," *Opt. Express* 21(2), 1440-1447 (2013).
- [3] Marsili, F., Verma, V. B., Stern, J. A., Harrington, S., Lita, A. E., Gerrits, T., Vayshenker, I., Baek, B., Shaw, M. D., Mirin, R. P., Nam, S.W., "Detecting single infrared photons with 93% system efficiency," *Nature Photon.* 7, 210-214 (2013).
- [4] Lusche, R., Semenov, A., Il'in, K., Korneeva, Y., Trifonov, A., Korneev, A., Hübers, H.-W., Siegel, M., Gol'tsman, G., "Effect of the Wire Width and Magnetic Field on the Intrinsic Detection Efficiency of Superconducting Nanowire Single-Photon Detectors," *IEEE Trans. Appl. Supercond.* 23(3), 2200205 (2013).
- [5] Marsili, F., Najafi, F., Dauler, E., Bellei, F., Hu, X., Csete, M., Molnar, R. J., Berggren, K. K., "Single-Photon Detectors Based on Ultranarrow Superconducting Nanowires," *Nano Lett.* 11(5), 2048-2053 (2011).
- [6] Ejmaes, M., Cristiano, R., Quaranta, O., Pagano, S., Gaggero, A., Mattioli, F., Leoni, R., Voronov, B., Gol'tsman, G., "A cascade switching superconducting single photon detector," *Appl. Phys. Lett.* 91, 262509 (2007).
- [7] Najafi, F., Mower, J., Harris, N. C., Bellei, F., Dane, A., Lee, C., Hu, X., Kharel, P., Marsili, F., Assefa, S., Berggren, K. K., Englund, D., "On-chip detection of non-classical light by scalable integration of single-photon detectors," *Nat. Commun.* 6, 5873 (2015).
- [8] Najafi, F., Dane, A., Bellei, F., Qingyuan Zhao; Sunter, K. A., McCaughan, A. N., Berggren, K. K., "Fabrication Process Yielding Saturated Nanowire Single-Photon Detectors With 24-ps Jitter," *IEEE J. Sel. Top. Quantum Electron.* 21(2), 3800507 (2015).
- [9] Hortensius, H. L., Driessen, E. F. C., Klapwijk, T. M., Berggren, K. K., and Clem, J. R., "Critical-current reduction in thin superconducting wires due to current crowding," *Appl. Phys. Lett.* 100, 182602 (2012).
- [10] Rosfjord, K., Yang, J., Dauler, E., Kerman, A., Anant, V., Voronov, B., Gol'tsman, G., Berggren, K., "Nanowire single-photon detector with an integrated optical cavity and anti-reflection coating," *Opt. Express* 14, 527-534 (2006).